Astron. Astrophys. 360, 1163–1169 (2000)

ASTRONOMY AND ASTROPHYSICS

Emerging flux as a driver for homologous flares

N.D.R. Ranns, L.K. Harra, S.A. Matthews, and J.L. Culhane

Mullard Space Science Laboratory, University College London, Holmbury St. Mary, Dorking, Surrey, RH5 6NT, UK

Received 15 November 1999 / Accepted 16 June 2000

Abstract. We present multi-wavelength observations of 2 M-class solar flares observed by SoHO and Yohkoh, which appear to be homologous. By examination of the flare loop morphology and footpoints we propose a schematic reconnection scenario of a two loop interaction in a quadrupolar magnetic configuration, for both flares (Machado 1983; Mandrini 1991). After the first flare, the combination of chance emergence of new flux at an opportune location and a subsequent flare, of the type described by Heyvaerts et al. (1977), form a new quadrupolar configuration in which the second flare occurred. Therefore though the two M-class flares are homologous by definition, they appear to conform to a scenario in which the preflare conditions are reformed after the first flare by emerging flux, rather than models which involve the continual shearing of a single magnetic structure.

Key words: Sun: flares

1. Introduction

The definition of homologous flaring (e.g. Woodgate et al. (1984)) states that, a) members of a series must have the same main footpoints, allowing for horizontal motions of the underlying structures, as defined by Hα or EUV kernels. They must also share the same general shape in the main phase, essentially including similar loop structures, as defined by Hα ribbons or Soft X-ray (SXR) images, and b) radio bursts in a series must show similar dynamic spectra.

Homologous flares are a particularly interesting phenomena that pose some challenging questions about the conditions that lead to flaring. For example, are the preflare conditions destroyed by the first flare? If they are, then how are these conditions rebuilt and if they are not destroyed, then what mechanism is responsible for the termination of the first event and the subsequent triggering of the second (Martres et al. 1984)?

Previous studies of homologous flares have centered around Hα observations. Martres (1989) classified three types of homologous flare according to time separation. The time separation classes are hours, days and rotations. Martres (1989) notes some important features of homologous flares occurring hours apart, namely that a) members of a flare series will most likely have a similar Hα importance, implying the importance is related to the flare site, and b) that the presence of a large spot is a necessary condition for a homologous flare series.

In this paper we study an example of two homologous flares, occurring hours apart, at multiple wavelengths to investigate the events which lead to the apparent homology. The data was obtained from the Yohkoh and SoHO spacecraft for AR8084 which was observed on the limb for a period of at least 10 hours on 17^{th} September 1997. During this period two M-class flares and one C-class flare occurred in this active region. We present evidence to support the hypothesis that the two M-class flares are homologous and that this homology stems from the fact that similar pre-flare conditions consisting of a quadrupolar magnetic configuration, were regenerated by the emergence of new flux. Sect. 2 details the observations taken of the active region. In Sect. 3 we examine the individual properties of the studied flares in the context of the adopted magnetic reconnection scenario. In Sect. 4 we discuss schematically the evolution of the active region as determined by the flaring activity and flux emergence. We discuss the results and their implications for homologous flares in Sect. 5.

2. Observations

This work is centered around images taken by the Yohkoh spacecraft with the Soft X-ray Telescope (SXT) and the Hard X-ray Telescope (HXT) onboard Yohkoh and with the Extreme Ultraviolet Telescope (EIT) and the Coronal Diagnostic Spectrometer (CDS) on board SoHO. The SXT is a grazing incidence telescope that forms X-ray images in the $0.25\,\mathrm{keV}$ to $4\,\mathrm{keV}$ range on a 1024 x 1024 CCD detector. A selection of metallic filters provides the capability to separate different X-ray energies for plasma temperature diagnostics (Tsuneta et al. 1991). The HXT is a Fourier synthesis imager of 64 elements which operates in the range $14\,\mathrm{keV}$ to $93\,\mathrm{keV}$. Each subcollimater measures a spatially-modulated incident photon count, which is Fourier-transformed into an image (Kosugi et al. 1991). The EIT is a full disk solar imager employing multilayer normal incidence extreme-ultraviolet optics to image the Sun in narrow temperature ranges, from chromospheric temperatures (He II $\approx 8 \times 10^4$K) to coronal temperatures (Fe XV $\approx 2 \times 10^6$K) (Delaboudinière et al. 1995). The CDS is a double spectrometer consisting of the Grazing Incidence Spectrometer (GIS) and the stigmatic imaging Normal Incidence Spectrometer (NIS). This enables CDS to cover a wide wavelength range

Send offprint requests to: N.D.R. Ranns (ndrr@mssl.ucl.ac.uk)

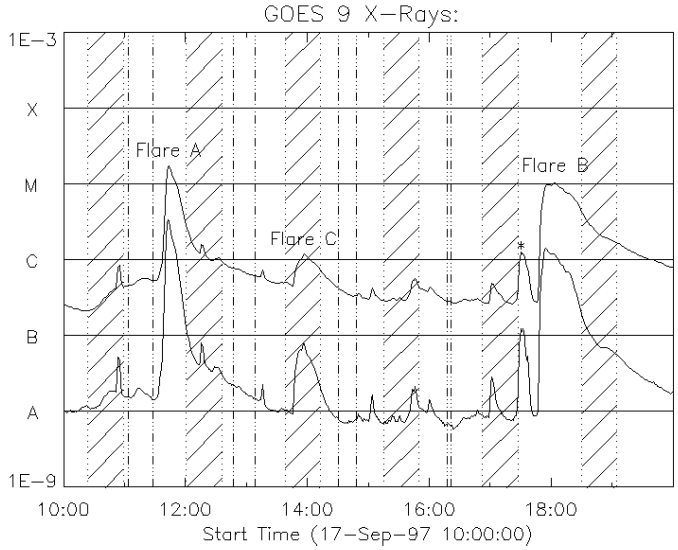

Fig. 1. GOES Light Curve of 17 September 1997, showing the three flares under study and the observing times of Yohkoh. Shaded areas mark the times of Yohkoh night. Regions between dot-dashed lines indicate satellite passage through the South Atlantic Anomaly (SAA). Flares marked with an asterisk did not occur in the active region under study. The EIT observations were continuous throughout the observing period. CDS observed the active region from 12:41UT until 15:55UT.

Table 1. The timing and GOES classification of the studied flares.

Flare Number	X-Ray Class	Start	Max
Flare A	M1.7	11:35	11:43
Flare B	M1.0	17:45	18:03
Flare C	C1.2	13:57	14:10

from $150 \rightarrow 800$ Å (Harrison et al. 1995). The CDS observations were taken by the NIS with the 4.06 arc-second slit. Each exposure time was 10 seconds and the field of view was approximately 240 arc-seconds square. The CDS-NIS generates images by rastering the slit across the target area resulting in one full image every 16 minutes. Images were taken in Fe XVI$_{\lambda 361}$, Si X$_{\lambda 347}$, Si X$_{\lambda 356}$, Mg IX$_{\lambda 368}$, O V$_{\lambda 629}$ and He I$_{\lambda 584}$ lines, covering a temperature range of approximately $2 \times 10^4 K$ to $2 \times 10^6 K$.

The following calibrations were applied to the data. For SXT the data were decompressed and the dark current and pin hole leak subtracted. Spikes from the data where then removed, the vignette correction applied and the images co-aligned. For EIT data the dark current was subtracted and the images degridded and flat-fielded. For CDS data the cosmic rays were removed and the data was compensated for the NIS CCD bias. Calibration to physical units of ergs cm^{-2} s^{-1} sr^{-1} Å^{-1} followed and finally corrections to remove the tilt and slant of the image on the detector were applied.

Fig. 1 shows the GOES SXR light curve for the observing period, with flares A, B and C indicated. Their start times, maximum times and SXR classes are listed in Table 1.

3. Individual flare properties

3.1. Flare A

The first flare in the series, Flare A, was classified as a GOES M1.7 event. Enhanced SXR emission measured by GOES began at 11:35UT and reached maximum emission at 11:43UT. The decay from maximum was initially fast, falling to a flux level of C1.6 by 12:10UT. The decrease in intensity was then more gradual taking another hour to fall to preflare levels.

Images from SXT during the pre-flare, impulsive and decay phases of flare A are shown in Fig. 2. The pre-flare image (Fig. 2a) shows an amalgamation of SXR structures located above latitude N30. The impulsive phase image (Fig. 2b) is dominated by a single bright SXR source, which is spatially coincident with the HXR source. This source is labeled Loop 3 and is located at the footpoint of the southern most part of the preflare structures. Fig. 2c shows an EIT Fe XII image taken during the impulsive phase. This image shows that the principal EUV source is also co-spatial with the SXR source.

The decay phase image (Fig. 2d) clearly illustrates the loop morphology of the active region that has arisen as a consequence of the flare. The pre-flare structure (Loop 1) has been heated and its density increased, by the flare and two new loops have appeared; one of similar size adjacent to Loop 1 (Loop 2), and another which spans the whole active region (Loop 4). The principal flare loop (Loop 3) which dominated the impulsive phase has faded.

In the corona the magnetic field pressure is greater than the plasma pressure, hence the magnetic field confines the plasma and the plasma structures can therefore be used as a tracer of the field structure, although the absolute directivity of the field cannot be determined. Since the active region is located on the limb we can determine to a high degree of certainty, using SXR observations, what magnetic loops are involved in the flare. We also use HXR and EUV observations of the footpoints to further clarify the location of individual loops. This technique to determine the schematic magnetic field structure and consequently a schematic reconnection scenario has been applied previously with success by a number of other authors (e.g. Woodgate et al. 1981, Inda-Koide et al. 1995, Nishio et al. 1997 and Aschwanden et al. 1999) and was also used for the detection of loop top Hard X-ray sources (Masuda et al. 1994).

The flare reconnection scenario that best describes the observations of Flare A, at X-ray and EUV wavelengths, is a quadrapolar reconnection scenario. Fig. 3 gives a schematic drawing of this envisaged reconnection scenario for Flare A. Reconnection at the separator of the two separatrix surfaces mapped out by the the merging pre-flare loops (Loops 1 and 2 in the above observation) forms the principal flare loop (Loop 3) in between their respective footpoints. The high altitude loop (Loop 4) is formed by the magnetic raking of coronal plasma by the field lines that are ejected upward from the reconnection site (Machado et al. 1983). A possible mechanism for the heating of the pre-flare loops is the injection of energetic particles from the reconnection site (Machado et al. 1983). This heating mechanism is further supported by the analysis of Flare B.

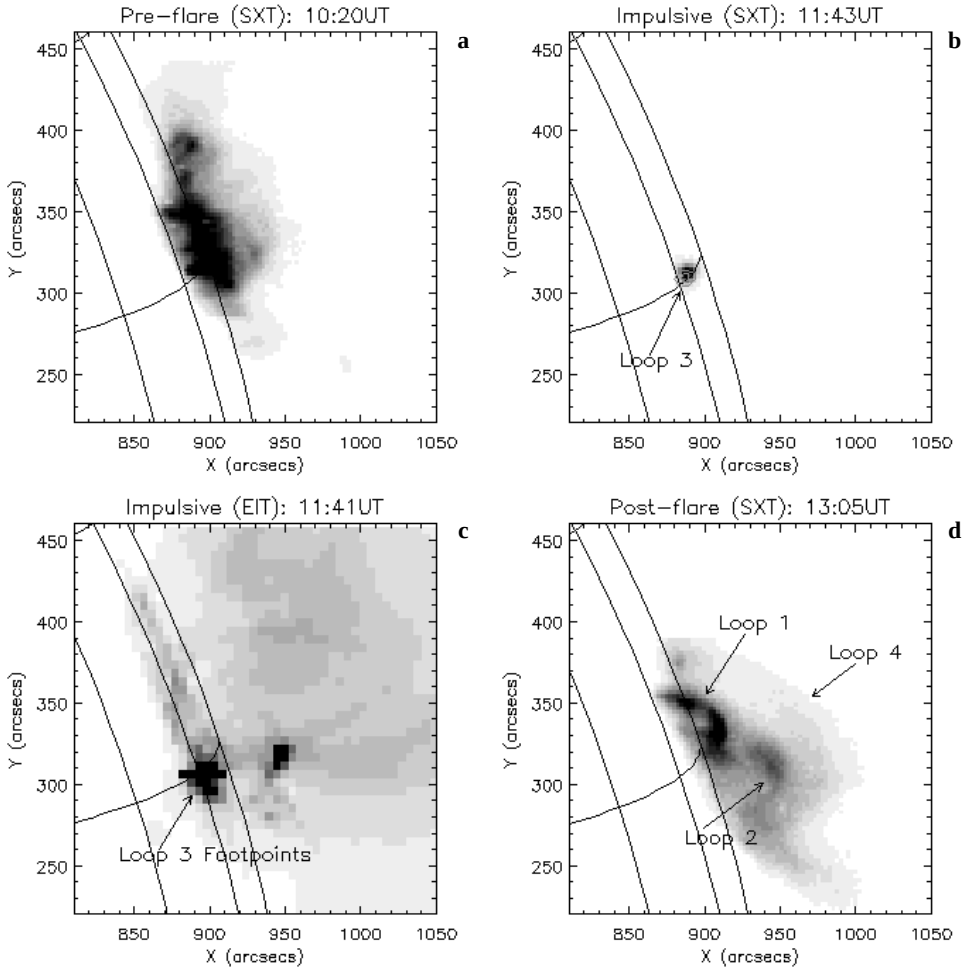

Fig. 2. a, **b** and **d** show SXT pre-flare, impulsive and decay phase images respectively of Flare A. On the impulsive phase image is contoured the HXR image. **c** shows an EIT Fe XII image taken during the impulsive phase. These images show that during the impulsive phase the principal SXR, HXR and EUV sources are co-spatial.

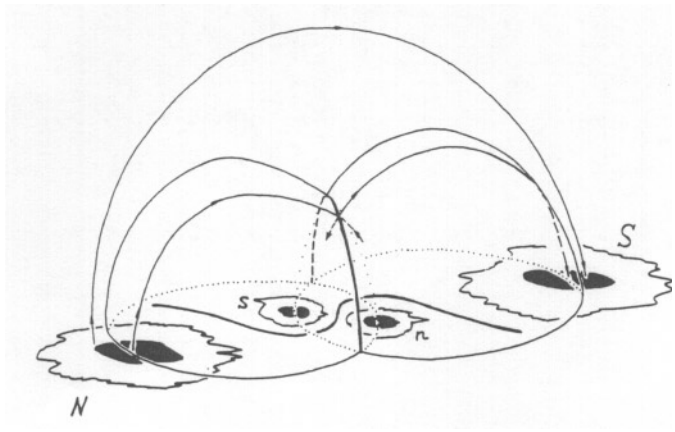

Fig. 3. The magnetic configuration believed to be in evidence in this case. This image is taken directly from Machado et al. 1983. This diagram is not to scale.

The occurrence of flares in a quadrapolar magnetic configuration is a well studied topic. The resulting reconnection scenario has also previously been successfully applied to disk observations of solar flares combined with magnetograms to explain such flare characteristics as Hα ribbons (Mandrini 1993; Démoulin et al. 1993; van Driel-Gesztelyi et al. 1994), chromospheric flare brightenings (Mandrini et al. 1995) and X-ray loop morphology (Machado et al. 1983).

3.2. Flare B

The second homologous flare in this series, Flare B, occurred at 17:45UT. The GOES lightcurve for this event (Fig. 1) shows a fast rise to maximum emission, less than 10 minutes, in both energy channels, followed by a much slower decline than displayed by Flare A, taking more than 3 hours to return to preflare flux levels. Fig. 4 shows pre-flare, impulsive and decay phase images of Flare B from SXT and EIT. In the pre-flare image the two separate loops are not clearly discernible. Similarly to Flare A the impulsive phase of Flare B (Fig. 4b) is dominated by a single SXR source that is located beneath the pre flare structure. This bright SXR source is again spatially coincident with the HXR source. A full resolution EIT observation (Fig. 4c) of the early impulsive phase, taken in FeXV, shows this emission clearly resolved as two sources. We interpret this emission as originating from the flare loop footpoints, based on the correlation of HXR and EUV emission which has been proven by many previous studies (e.g. Kane et al. 1980). This implies that the central source is indeed an unresolved loop. There is also a smaller HXR source in the impulsive phase images located at

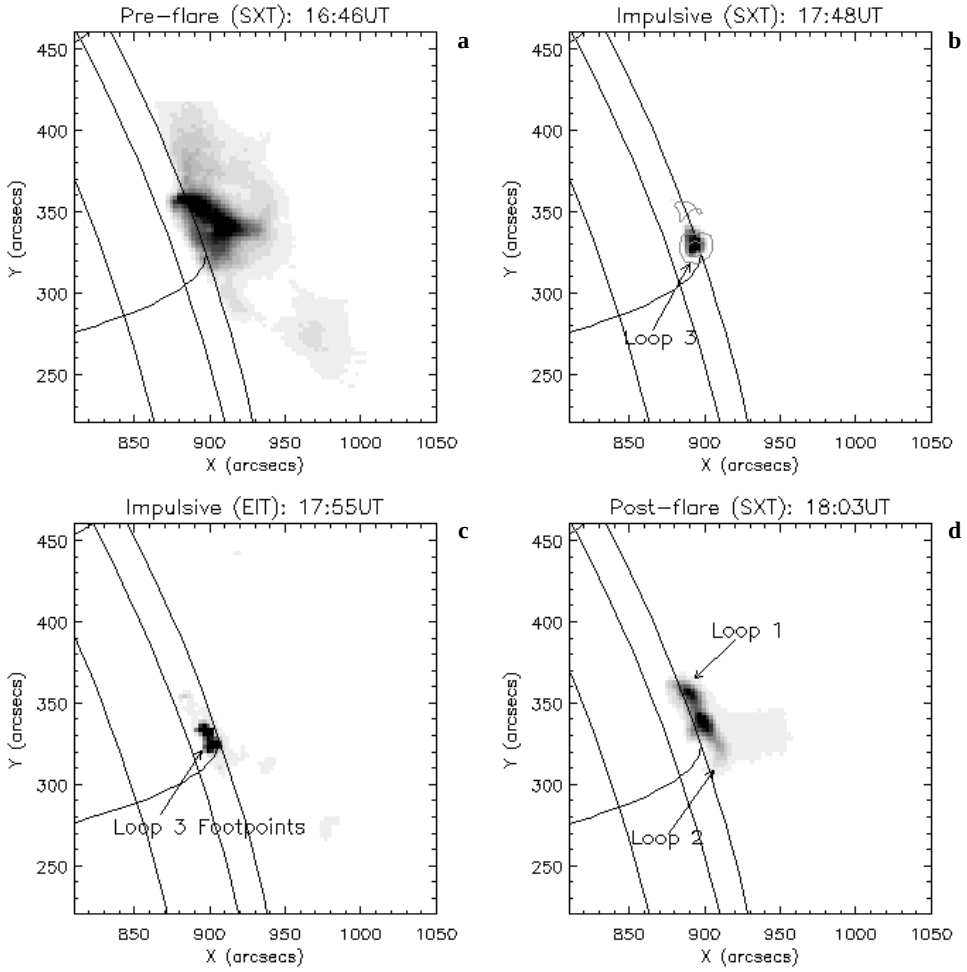

Fig. 4a–d. Yohkoh and EIT observations of the pre-flare **a**, impulsive **b**, **c** and decay **d** phases of Flare B. The HXR image is contoured on the impulsive phase image at 17:50UT.

the footpoint of the northern flare loop (Loop 1). This suggests the presence of energetic particles in the loop accounting for its heating and filling via chromospheric evaporation. Allowing for rotation the main SXR sources of Flares A and B appear co-spatial to within the resolution of SXT.

The decay phase image (Fig. 4d) shows a very similar loop morphology to that of flare A in that two small loops connecting the intermediate dipole to the outer poles lie beneath a larger structure which connects the two outer poles. The flare loops are labeled similarly to those in the images of Flare A to highlight the comparisons.

3.3. Flare C

In the interim period between the two homologous flares A and B, a smaller C-class flare occurred at 14:10UT. The impulsive phase of Flare C occurred during Yohkoh night so SXR and HXR images are not available. However, SoHO-CDS was observing this active region and imaged the impulsive phase of this flare. Fig. 5a shows a Yohkoh pre-flare image in which the flare loops of the preceding M-class flare (Flare A), can be seen in addition to a new loop. This new loop was continually brightening until the cessation of Yohkoh observations at 13:46UT.

The flare occurs at the interaction point between the emerging loop and the pre-existing loop (Loop 1) and is manifested by an impulsive brightening in all CDS lines (He I, O V, Mg IX, Si X and Fe XVI) at the interaction point or the two loops. Brightenings at the footpoints of these two interacting loops are also visible in O V and He I. Fig. 5b shows again the SXR pre-flare image on which is contoured features seen in the impulsive phase by CDS. Post-flare images show the presence of two loops formed at the site of the pre-flare loops and a bright source above these loops. These newly formed loops connect the footpoints of the pre-existing loops to the footpoints of the recently emergent loop. For this flare the observational evidence supports a different reconnection scenario, namely that of an emerging loop interacting and subsequently reconnecting with a pre-existing loop, as described by Heyvaerts et al. (1977, hereafter HPR). The presence of emerging flux is hence assumed by the application of the HPR model.

4. Active region evolution

The suggested evolution of the active region is shown schematically in Fig. 6. The magnetic configuration has been inferred in the absence of magnetograms by the connectivity of the magnetic loops. In the corona $\beta \ll 1$ hence the plasma is con-

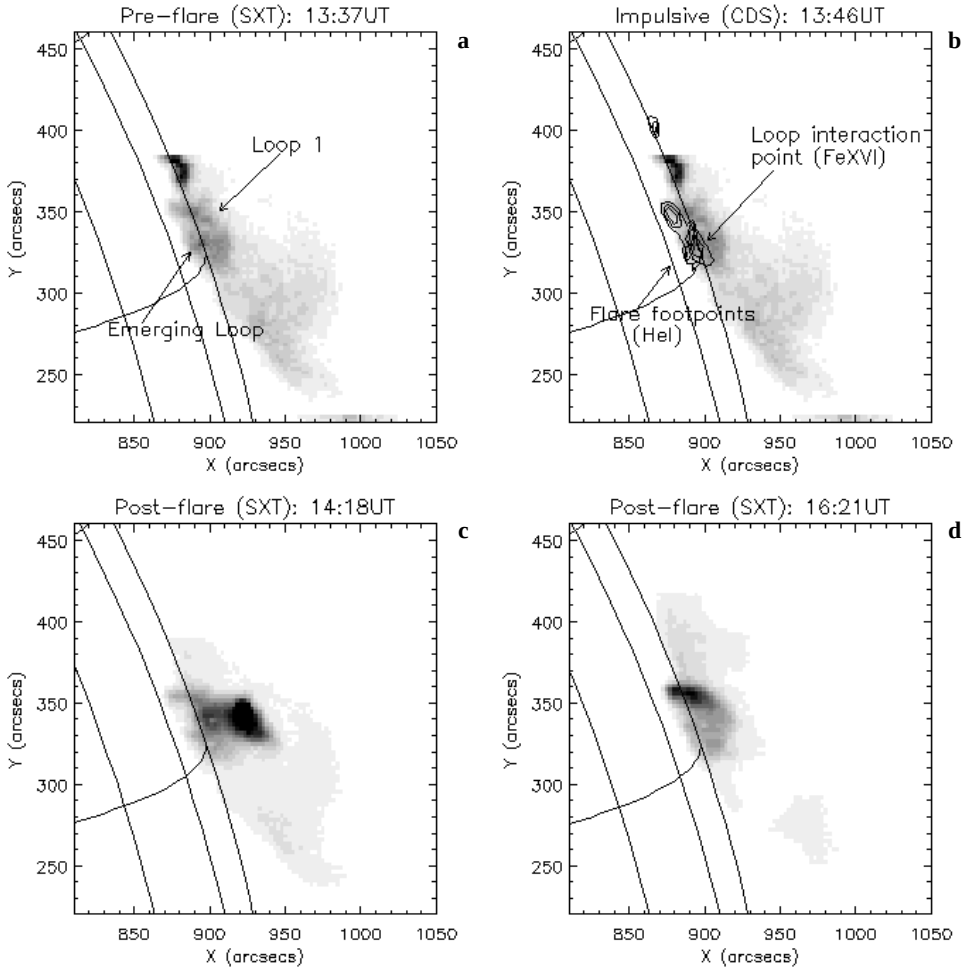

Fig. 5a–d. Yohkoh-SXT and CDS images of the pre-flare, impulsive and decay phases of Flare C.

fined by the magnetic field and can consequently be used as a tracer for magnetic field lines. Before Flare A the active region had an inferred magnetic configuration of the plus-minus-plus-minus type (Fig. 6a) with Loop 1 connecting footpoints W and X. Flare A occurred within this initial configuration through reconnection between Loops 1 and 2, creating the Loops 3 and 4 by the mechanism described in the preceding section (Fig. 6b). The emergence of a new loop below Loop 1 (Fig. 6c) and subsequently Flare C regenerates a similar quadrupolar magnetic configuration on a smaller scale (Fig. 6d) to that present before Flare A (Fig. 6a). This new quadrupolar magnetic configuration is then the site of Flare B (Fig. 6e).

Examination of photospheric magnetograms of this active region before it approached the limb revealed that the region was complex. Fig. 7 shows an MDI magnetogram from 20:00UT on the $15^{\rm th}$ of September a time when the Active Region was within 60° of disk center, the limit of a magnetograms longitudinal extent. This magnetogram shows that the region does indeed possess a quadrapolar magnetic configuration. Examination of a series of magnetograms up to the 15^{th} of September shows magnetic flux emergence. Both these characteristics of the photospheric magnetograms support our interpretation of the flares within the active region.

5. Conclusions

We have presented multi-wavelength observations of two similar flares (A and B) that occurred approximately 6.3 hours apart. They occurred in the same active region, displayed the same essential four part loop structure during the main phase, certainly share some common footpoints and, within the resolution of SXT, appear to share the same principal flare footpoints. They were also of similar GOES SXR magnitude. Therefore according to the literature definition, cf. Woodgate et al. 1984, these flares could therefore be classed as homologous.

In this example it is shown that the pre-flare configurations for both homologous flares (A and B) are quadrupolar magnetic configurations. Using multi-wavelength data we have made a careful study of the events occurring between the homologous flares and we propose that an interim flare (Flare C) caused by the reconnection of emerging flux and a pre-existing loop regenerated a quadrupolar configuration on a smaller scale that becomes the site of the second homologous flare. Therefore in reference to the question posed in Sect. 1, are the pre-flare conditions rebuilt after the first flare or is their a mechanism responsible for stopping the first event and triggering the second, these results support the hypothesis that the pre-flare conditions

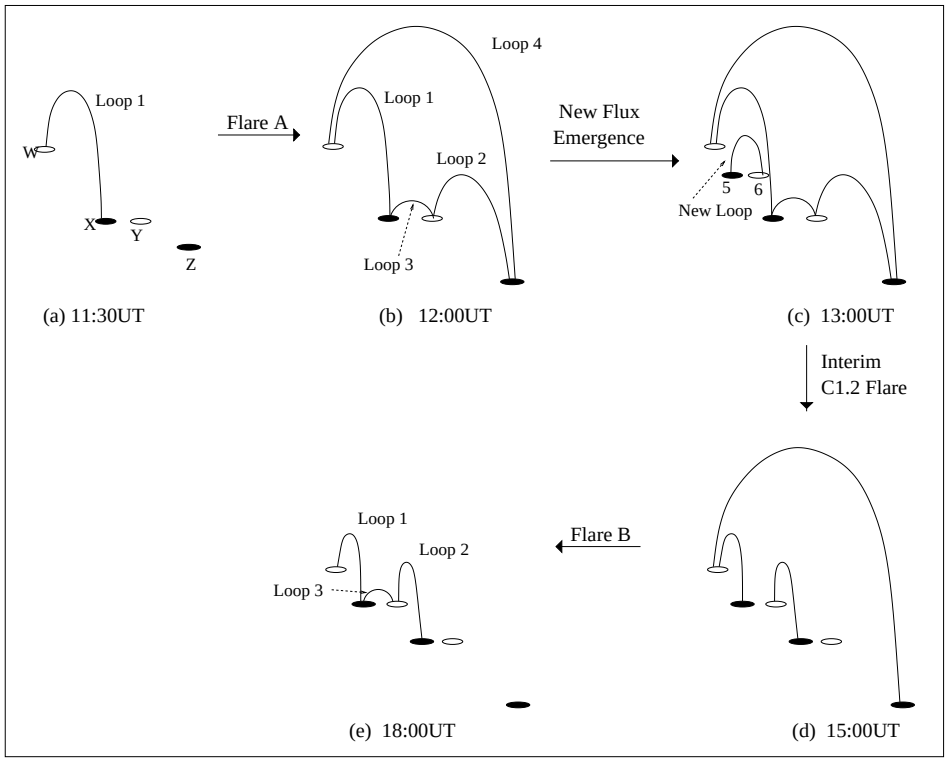

Fig. 6a–e. The inferred magnetic evolution of the active region. No information of the size of each spot is known so all spots are displayed as the same size. SXR loops are shown when they first appear and are labeled when they are first identified as part of a flare. When the loops are no longer visible within the system they are not drawn.

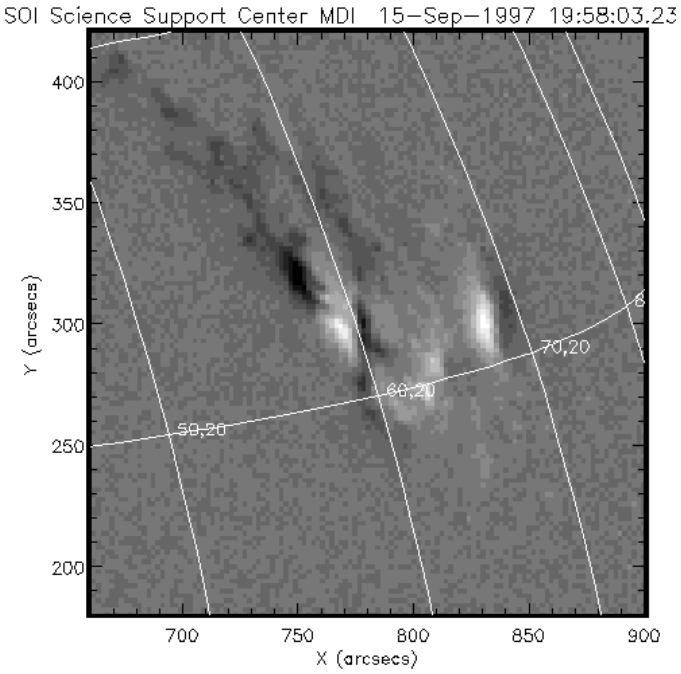

Fig. 7. An MDI photospheric magnetogram from 20:00UT September 15^{th}, showing the existence of a quadrapolar magnetic configuration.

appear to be destroyed but are rebuilt by the emergence of new flux.

Previous models that have addressed homologous flares have involved the continual stressing or shearing of a single, or group of, magnetic structures (Woodgate et al. 1984; Shibata 1998; Choe & Cheng 2000) and the importance of shear in producing flares in a quadrapolar region has also been shown (Karpen et al. 1995, 1998). However, although these flares fit the literature definitions of homology they appear to conform better to the above posed scenario rather than the continual shearing of a single magnetic structure. Thus we believe this is a different type of homology to previously studied examples.

With the continual advancements in image resolution, at all wavelengths, we are learning progressively more about the morphology and the mechanisms behind solar flares. Our results suggest the possibility that other conditions similar to the one described here, may exist to explain the production of apparently homologous flares.

Acknowledgements. NDRR, SAM and LKH acknowledge the finanical support of PPARC for a studentship, postdoctral post, and an advanced fellowship respectively. The authors would also like to thank the referee for improving the clarity of the paper.

References

Aschwanden, M. J. 1999, ApJ, 526, 1026
Choe, G. G., Cheng, C. Z., 2000, Submitted to ApJ.
Delaboudinière, J. -P., Artzner, G. E., Brunaud, J. et al., 1995, Solar Physics, 162, 291
Démoulin, P., van Driel-Gesztelyi, L., Schmieder, B. et al., 1993, A&A, 271, 292
Harrison, R. A., Sawyer, E. C., Carter, M. K. et al., 1995, Solar Physics, 162, 233
Heyvaerts, J., Priest, E. R., Rust, D. M., 1977, ApJ, 216, 123
Inda-Koide, M., Sakai, J-I., Koide, S. et al., 1995, PASJ, 47, 323
Karpen, J. T, Antiochos, S. K. and DeVore, R. C., 1995, ApJ, 450, 422
Karpen, J. T, Antiochos, S. K., DeVore, R. C. and Golub, L., 1998, ApJ, 495, 491

Kane, S. R., Lianell, L. J., Datlowe, D. et al., 1980, Solar Flares, editor Sturrock, P. A., p187
Kosugi, T., Makishima, K., Murakami, T. et al., 1991, Solar Physics, 136, 17
Machado, M. E., Somov, B. V., Rovira, M. G., de Jager, C., 1983, Solar Physics, 85, 157
Mandrini, C. H., Démoulin, P., Henoux, J. C., Machado, M. E., 1991, A&A, 250, 541
Mandrini, C. H., Rovira, M. G., Démoulin, P. et al., 1993, A&A, 272, 609
Mandrini, C. H., Démoulin, P., Rovira, M. G. et al., 1995, A&A, 303, 927
Martres, M. J., 1989, Solar Physics, 119, 357
Martres,M.-J., Mein, N., Mouradian, Z. et al., 1984, Advances in Space Physics Research, Vol.4, No.7, p5
Masuda, S., Kosugi, T., Hara, H. et al., 1994, Nature, 371, 495
Nishio, M., Kentaro, Y. Kosugi, T. et al., 1997, ApJ, 489, 976
Shibata, K., 1998, Five Years of Yohkoh and Beyond, editors Watanbe, T., Kosugi, T., Sterling, A. (eds), p187
Tsuneta, S., Acton, L., Bruner, M. et al., 1991, Solar Physics, 136, 37
van Driel-Gesztelyi, L.,Hofmann, A., Démoulin, P. et al., 1994, Solar Physics, 149, 309
Woodgate, B. E., Shine, R. A., Brandt, J. C. et al., 1981, ApJ, 244, L133
Woodgate, B. E., Martres, M.-J., Smith, J. B. et al., 1984, Advances in Space Physics Research, Vol.4, No.7, p11